Oxygen Embrittlement Kinetics at 500–600 °C of the Ti–6Al–4V Alloy Fabricated by Laser and Electron Powder Bed Fusion

Antoine Casadebaigt, Daniel Monceau, Jonathan Hugues

Oxygen embrittlement kinetics at 500 – 600 °C of the Ti-6Al-4V alloy fabricated by Laser and Electron Powder Bed Fusion

Antoine Casadebaigt[a,b], Daniel Monceau[b,*] Jonathan Hugues[a]

[a] IRT Saint Exupéry, 3 rue Tarfaya, 31405 Toulouse Cedex 4, France

[b] CIRIMAT, Université de Toulouse, CNRS, INPT, UPS, ENSIACET, 4 allée Emile Monso BP-44362, 31030 Toulouse Cedex 4, France

*corresponding author : daniel.monceau@toulouse-inp.fr

Abstract

Ti-6Al-4V alloys manufactured by laser or electron powder bed fusion (L-PBF and E-PBF) with or without hipping treatment have different microstructures from foundry alloys. Their oxidation kinetics at high temperatures between 500°C and 600°C for durations up to 2000 h were compared. The effect of oxidation on their room temperature tensile embrittlement was quantified. It was shown that the growth kinetics of the brittle fracture zone, of the zone with cracks at 1% strain, and of the oxygen diffusion zone were perfectly correlated. Therefore, the embrittlement was confirmed to be due to oxygen ingress below the oxide scale and the kinetics were independent of the microstructure.

Keywords

Titanium alloy, embrittlement kinetics, oxygen diffusion, additive manufacturing, Ti-6Al-4V

Introduction

Titanium alloys are used in aeronautic, ~~aerospace,~~ energy or biomedical fields due to their high specific mechanical properties and resistance to corrosion at room temperature. The past twenty years, the number of studies about additive manufacturing (AM) of metals parts has increased [1, 2]. These new processes, such as Laser Powder Bed Fusion (L-PBF) and Electron Powder Bed Fusion (E-PBF) allow breaking down previous technological barriers thanks to the ability of producing parts, which could not be made by conventional processes such as casting and rolling or forging. Concerning AM of titanium alloys, most published studies focuses on alloy Ti-6Al-4V [3]. Many studies show that thin acicular α’ and lamellar α + β microstructures

of L-PBF and ~~EBM~~ E-PBF Ti-6Al-4V, respectively, can achieve similar or better mechanical properties at room temperature than for conventionally processed alloys [4-6]. The Hot Isostatic Pressing (HIP) treatment is frequently used on AM parts to close pores and to improve alloy ductility and fatigue properties [3, 6].

Titanium alloys are also intended to be used at high temperatures, replacing steels or nickel-based superalloys, with the goal of reducing mass. This is the case in gas turbines, which see their operating temperature constantly increasing leading to higher oxidation rates. High temperature oxidation of titanium alloys is characterized by the formation of an external oxide layer and of an oxygen diffusion zone (ODZ) beneath it~~, called ODZ~~. Indeed, metals such as titanium, zirconium or hafnium, have a very high solubility of oxygen. This interstitial element affects mechanical properties [7]. Oxygen, and other interstitials such as nitrogen, hydrogen and carbon strengthens the metal, but also induces a change from ductile to brittle rupture mode in areas where these interstitials are present in large enough concentrations [7-9]. The formation of cracks at the surface of oxidized specimens was observed under tensile stress [10-12]. Shamblen *et al.* [11], Bendersky *et al.* [10] and Evans *et al.* [13] observed the formation of cracks along the surface of pre-oxidized Ti6242s and IMI834 specimens during tensile and creep tests, respectively. They noticed the increase in crack length with oxidation duration. Texier *et al.* removed the oxide layer of oxidized specimens in order to only keep the ODZ and observed the formation of horizontal cracks in the ODZ [14]. Bendersky *et al.* [10], Leyens *et al.* [15] and Jia *et al.* [12] observed that these cracks correspond to a brittle rupture mode of the oxygen diffusion zone. The presence of cracks then decreases the strain at rupture of the tensile specimen at room temperature. Other studies [11, 16-18] also observed this modification of the rupture mode and compared the thickness of the brittle rupture zone in oxidized specimens with the oxygen concentration profile. It showed that the oxygen diffusion zone can be evaluated differently depending on the characterisation method. However, Pilchak *et al.* [19] characterized the oxygen diffusion zone of Ti6242S alloy with four different methods and observed small differences in oxygen diffusion zone lengths. These four methods were oxygen concentration profile measurement with EPMA, observation of a white layer with an optical microscope or observation after oxalic etching and realization of microhardness profiles.

Texier *et al.* studied the influence of oxidation at 750 °C on Ti-6Al-4V titanium alloy mechanical properties on thin specimens in order to increase surface/volume ratio [14]. They showed that the thinner the sample, the shorter the oxidation time needed to embrittle the sample and to have a totally brittle fracture. One use of AM processes is to build parts with thin walls

in order to decrease their mass. However, thin walls have a high surface/volume ratio, which may greatly increase oxygen embrittlement. A few studies characterized the high temperature oxidation of titanium alloys fabricated by additive manufacturing. These works reported that additively manufactured titanium alloys have similar or lower oxidation kinetics as conventionally processed ones [20-26]. However, to the knowledge of the authors, no work has been devoted to the effect of oxidation on the mechanical properties of titanium specimens resulting from additive manufacturing, but the influence of interstitials on the mechanical behaviour has been observed [27]. In the present work, the oxygen embrittlement of L-PBF and ~~EBM~~ E-PBF Ti-6Al-4V specimens oxidized at 500, 538 and 600 °C is characterized and compared to the embrittlement of conventionally processed Ti-6Al-4V alloys. The kinetics of embrittlement are determined. Quantitative correlations are established between the kinetics of growth of the ~~oxygen diffusion zone (~~ODZ~~)~~ measured with electron microprobe (EPMA) or using microhardness profiles and the kinetics of growth of the brittle zone as observed by fractography or by observation of the depth of cracks after interrupted tensile tests.

Materials and Experimental procedures

Ti-6Al-4V alloys samples fabricated by ~~Laser Powder Bed Fusion and Electron Powder Bed Fusion~~ L-PBF and E-PBF were studied and compared to conventionally processed samples (cast and rolled). EOS M280 machine located at FUSIA, France and equipped with an Yb-Fibre laser was used to fabricate L-PBF samples. Standard EOS parameters for Ti-6Al-4V were used to obtain fully dense parts. L-PBF processing was carried out under Ar atmosphere with concentrations below 3.0 ppm of O_2, 10 ppm of N_2 and 1 ppm of H_2O. AP&C plasma atomised Ti-6Al-4V grade 23 powder, with a particle size of 15 - 45 µm was used. Arcam Q20+ machine located at IRT Saint Exupéry, France and equipped with a LaB_6 cathode was used to fabricate ~~EBM~~ E-PBF samples with Arcam parameters and theme 5.2.24, in vacuum atmosphere under 4.10^{-3} mbar of He. AP&C plasma atomised Ti-6Al-4V grade 23 powder, with a particle size of 45 - 106 µm was used. Chemical composition of powders used for L-PBF and ~~EBM~~ E-PBF fabrication were presented in a former work [24]. L-PBF and ~~EBM~~ E-PBF samples, with chemical composition presented in Table 1, were compared to conventionally processed Ti-6Al-4V grade 5, presenting an oxygen level up to 0.2 wt%. Some of L-PBF samples were annealed at 720 ± 5 °C for 2 h +20/-0 min to relieve residual stresses and avoid deformation during the cut of samples from the building platform. Some of the L-PBF and ~~EBM~~ E-PBF samples were submitted to HIP treatment at 920 ± 10 °C and 1020 ± 20 bars for 2 h + 24/- 0

min under Ar atmosphere with 1.0 ppm of O_2, 1.5 ppm of N_2 and 4.6 ppm of H_2O at Bodycote, France.

Table 1: Chemical composition of Ti-6Al-4V alloys used in this study (measured by Instrumental Gas Analysis (IGA) for O, N, H and C and Inductively Coupled Plasma-Optical Emission Spectrometry (ICP-OES) for Al, V, Fe, Cr and Ti

	Al	V	Fe	Cr	O	N	H	C	Others	Ti
	%	%	%	%	ppm	ppm	ppm	ppm	%	
As-built L-PBF (wt% or ppm)	5.99 ± 0.02	4.00 ± 0.02	0.2 ± 0.002	<0.05	1000	100	30	100		Bal
As-built ~~EBM~~ E-PBF (wt% or ppm)	5.59 ± 0.02	4.01 ± 0.01	0.19 ± 0.003	<0.05	800	140	10	100		Bal
Rolled β-annealed (wt% or ppm)	6.41	3.93	0.16		1800	100	40	40	< 0.4	Bal

Microstructure characterisations were performed on cross-sections, by optical (OM) and Scanning Electron Microscopies (SEM). Cross-sections were ground up to P2400 - SiC abrasive paper and polished with a SiO_2 solution. Characterisation's procedures were described in a former work [24]. SEM and OM observations of as-built L-PBF, L-PBF and annealed, ~~EBM~~ E-PBF and HIP treated, as-built ~~EBM~~ E-PBF, ~~EBM~~ E-PBF and HIP treated, rolled β and annealed, and cast β annealed are presented in Fig. 1**.** As-built L-PBF microstructure is composed of acicular α'-martensite, with the largest laths thickness being about 0.6 ± 0.1 µm. Annealing and HIP thermal treatments performed on as-built L-PBF induces the formation of α-laths into a β-matrix. α-laths thickness is about 0.5 ± 0.2 µm for L-PBF annealed and about 2.4 ± 1.2 µm for L-PBF HIP treated. As-built ~~EBM~~ E-PBF and ~~EBM~~ E-PBF HIP treated microstructures are both composed of α-laths into a β-matrix with α-laths thickness of 0.7 ± 0.2 µm and 2.5 ± 0.4 µm, respectively. α_{GB} phase was also observed on ~~EBM~~ E-PBF HIP treated sample with a thickness close to 1 µm. For rolled and cast Ti-6Al-4V, microstructures are both α-laths into a β-matrix with α-laths thickness of 1.0 ± 0.3 µm and 2.0 ± 0.3 µm, respectively. Moreover, the two former microstructures present thick α_{GB} phase at the grain boundaries with a thickness of 3.5 ± 0.5 µm and 6.1 ± 1.3 µm, respectively.

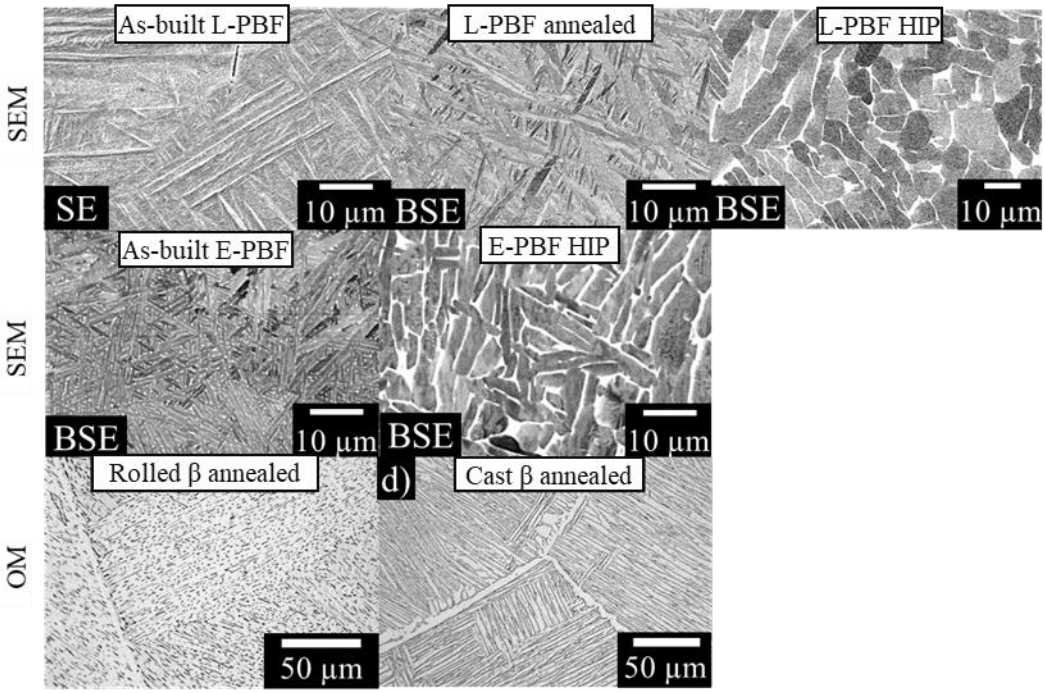

Figure 1: Scanning electron and optical microscopies of additively manufactured and conventionally processed Ti-6Al-4V alloys

In order to study the influence of microstructure on oxidation behaviour, **33** samples were fabricated by L-PBF, **33** samples by ~~EBM~~ E-PBF and **one** sample was rolled β-annealed. L-PBF and ~~EBM~~ E-PBF samples size was 28 x 28 x 2 mm^3 and rolled β-annealed sample size was 15 x 10 x 2 mm^3. **19** L-PBF (L-PBF P600), **19** ~~EBM~~ E-PBF (~~EBM~~ E-PBF P600) and **one** rolled β-annealed (rolled P600) samples were ground with P600 – SiC abrasive paper. **14** L-PBF (L-PBF HIP P600), **14** ~~EBM~~ E-PBF (~~EBM~~ E-PBF HIP P600) samples were HIP-treated and ground with P600 – SiC grinding paper. Each sample was cleaned in acetone and then in ethanol in an ultrasonic bath for 1 min prior to oxidation.

Oxidation treatments were carried out at 500, 538 and 600 °C, for different durations ranging from 25 to 5 000 h. Sample mass was measured before and after oxidation using an electronic balance Sartorius LA 75 3200D with an accuracy of ± 20 µg. Net mass change per unit area (mass gain) values were averaged on three to five measurements for each oxidation test. More details on the oxidation test procedure can be found in [24].

Oxide layer (OL) characterisations were performed on cross sections with a Nikon Eclipse OM and a FEI Quanta 450 SEM at CIRIMAT, France, and a SEM/FIB HELIOS 600i at the R. Castaing Microanalysis Centre, France. OL thickness was determined by averaging 10 to 150 measures depending on oxidation conditions.

The ~~Oxygen Diffusion Zone (~~ODZ~~)~~ was characterised by ~~Electron Probe Microanalyzer (~~EPMA~~)~~ with a CAMECA SXFive FE operating at 15kV and 20 nA at R. Castaing Microanalysis Centre, France. For each sample characterized, 3 to 6 concentration profiles were measured. Due to the presence of a native oxide layer on the surface of the freshly polished cross section, the oxygen signal was biased of about 4 wt.% of oxygen and had to be corrected. For each profile, three count values were measured in the bulk to determine the count value corresponding to the native OL. The mean value of the bulk was brought back to zero because the machine error of measured points is six times higher than the oxygen concentration in the bulk. Then, oxygen concentrations in at.% and wt.% were calculated from the remaining intensity counts. The effective diffusion coefficient of oxygen (D) in the metal was experimentally determined by fitting EPMA profiles with Fick's second law, **Eq 1**, with the oxygen concentration at the metal/oxide interface, C_s (at%), the oxygen concentration in the bulk, C_0 (at%), the oxygen at the depth x (m), C_x (at%,), the oxidation time, t (s), and D in m^2/s, being constant.

$$\boldsymbol{C_x = C_0 + (C_s - C_0) \cdot \left(1 - erf\left(\frac{x}{2\sqrt{D \cdot t}}\right)\right)} \qquad \text{Eq.1}$$

To determine the ODZ_{EPMA} thickness, the criteria $\boldsymbol{ODZ = 4\sqrt{D \cdot t}}$ was chosen, based on the ratio $\boldsymbol{\frac{(C_x - C_0)}{(C_s - C_0)} \approx 0.005}$ as presented in **Eq 2**, and shown in **Fig**. 10 by Casadebaigt *et al.* work **[24]**.

$$\boldsymbol{\frac{(C_x - C_0)}{(C_s - C_0)} = 1 - erf(2) \approx 0.005} \qquad \text{Eq.2}$$

This criteria corresponds to the metal thickness value for which an oxygen concentration is about 0.5 at.% for most samples. The use of $\boldsymbol{4\sqrt{D \cdot t}}$ is thought to be better than an "assessment with the eyes" of the oxygen diffusion length from the EPMA plots. It has the advantage of being independent of the operator.

Tensile tests were performed at room temperature on a MTS Criterion at MIDIVAL, France using a high temperature Epsilon extensometer with a 20 mm working distance to measure displacement. Tensile specimens were fabricated by L-PBF and ~~EBM~~ E-PBF parallel

to the manufacturing direction and machined with a gauge area of 30 x 5 mm², a thickness of 1.3 mm and were ground with P600–SiC grinding paper. In order to investigate the influence of microstructure and oxidation on tensile properties, L-PBF annealed, L-PBF HIP treated, ~~EBM~~ E-PBF, ~~EBM~~ E-PBF HIP treated and cast Ti-6Al-4V specimens were compared. Tensile specimens were oxidized for 500, 1 000 and 2 000 h at 500 °C and 538 °C and for 100, 200, and 500 h at 600 °C for different durations in a Carbolite furnace LHT6/60 with forced air convection before running tensile tests. For each oxidation condition, three specimens were tested in order to assess the repeatability of tensile properties. Strain was measured with an extensometer in the gauge area. Tensile tests were performed with a strain rate of 5.10^{-3} s^{-1} up to 1.2 % of total strain. After 1.2 % of total strain, strain rate was increased to 5.10^{-2} s^{-1} as detailed in ASTM E 0008. Surand showed that Ti-6Al-4V has a dependency to the strain rate [28]. However, in our work, all tensile tests were performed with the same testing conditions, supposing that the modification of strain rate should not interfere with the study of the influence of oxidation on tensile properties. The rupture surface of oxidized tensile specimens was observed using a LEO 435 VP SEM. Cross sections of ruptured oxidized tensile specimens were prepared and ground up to P2400 SiC paper and polished with SiO_2 solution.

Results

After performing the tensile tests at room temperature, brittle rupture was observed on the surface of tensile specimens and ductile rupture was observed in the bulk, for ~~EBM~~ E-PBF, cast and L-PBF specimens, **Fig. 2**. Brittle rupture zone thickness (ODZ_{Br}) was averaged from the measures at 40 to 80 locations for each specimen.

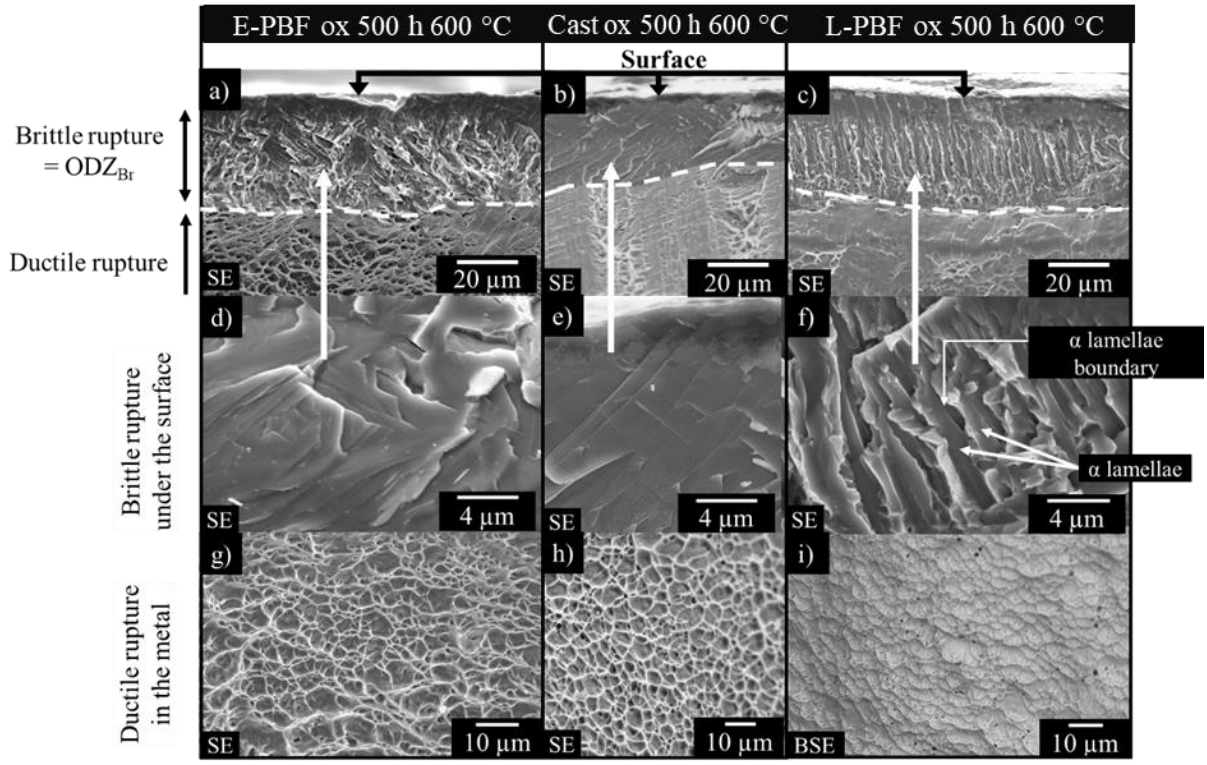

Figure 2 : Observation by SEM of rupture surfaces of ~~EBM~~ E-PBF P600, cast and L-PBF P600 specimens oxidized 500 h at 600 °C. Brittle rupture depths were measured on similar SEM images.

Cross sections of ruptured oxidized tensile specimens showed the presence of opened cracks on the surface of specimens along the tensile specimens, **Fig. 3.** These cracks correspond to the ODZ_{Br} observed on the rupture surface, **Fig. 2**. Crack's length (ODZ_{Cr}) was measured along the tensile specimens and the average on 100 measured cracks' lengths was calculated for each oxidized tensile specimen.

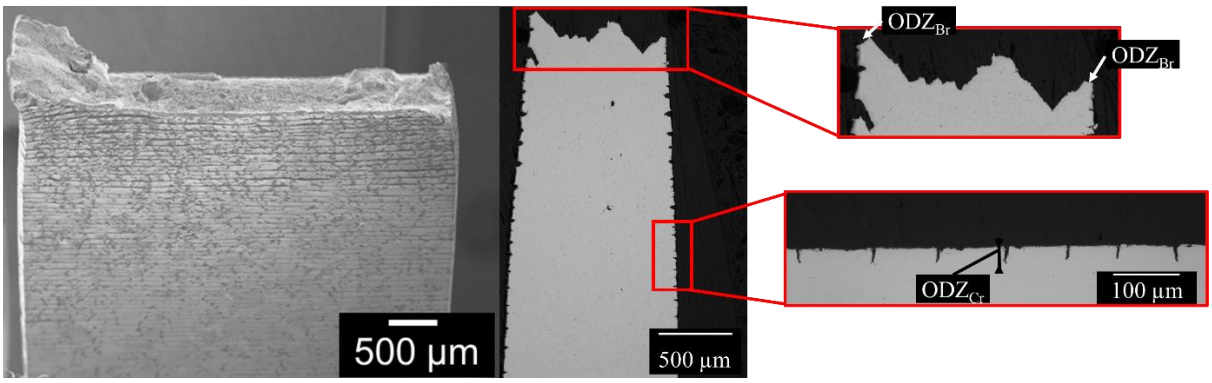

Figure 3: SEM observation and cross section of ~~EBM~~ E-PBF P600 ruptured tensile specimens oxidized 500 h at 600 °C. Measure of crack depth along the tensile specimen.

Interrupted tensile tests were performed to determine when the formation of cracks occurs on tensile specimens oxidized 500 h at 600 °C, **Fig. 4**. Three cast β annealed P600 tensile specimens, oxidized 500 h at 600 °C, were tested up to 0.3, 0.5 and 1.0 % of total strain. For each specimen, a cross section was prepared to see if residual cracks were present after the loading and unloading of the specimens. At 0.3 and 0.5% strain, no cracks were present whereas at 1.0% strain, cracks were present in the ODZ. For cast β-annealed P600 tensile specimens oxidized 500 h at 600 °C, cracks were formed before 1% strain in the gauge area.

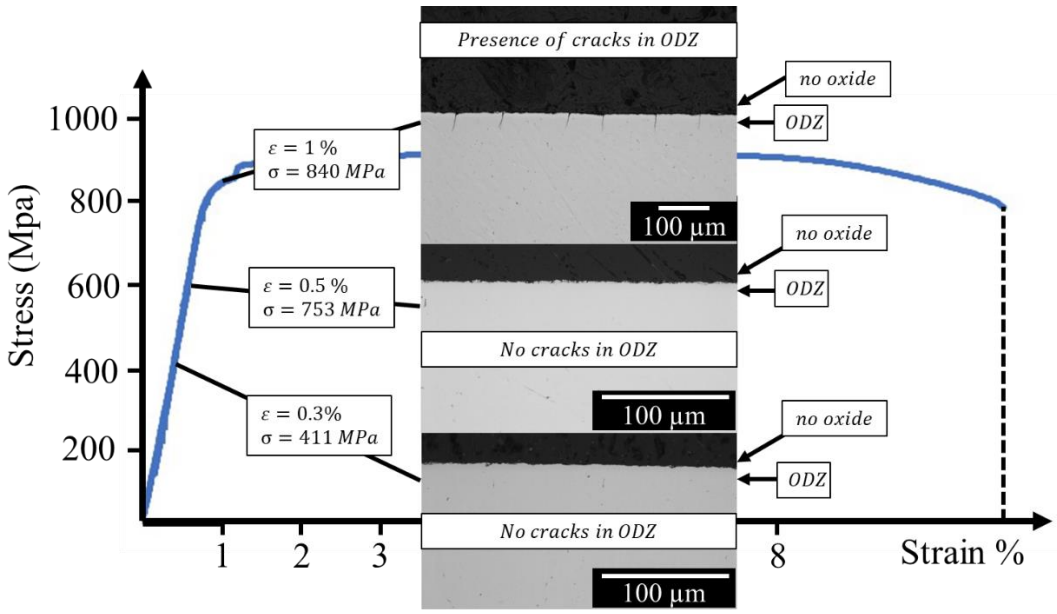

Figure 4 : Interrupted tensile tests performed up to 0.3, 0.5 and 1 % strain on cast Ti-6Al-4V oxidized 500 h at 600 °C, with corresponding cross section of unloaded tensile specimens showing the presence of cracks in the ODZ at 1% strain.

~~In the preceding part, we have defined several parameters that define how much the alloy is affected by the environment, i.e. the oxide layer thickness (OL), the oxygen diffusion zone measured by EPMA (ODZ_{EPMA}), the layer embrittled by oxygen (ODZ_{Br}), the layer with a network of fractures perpendicular to the applied force (ODZ_{Cr}). In the following, we will describe how these parameters OL, ODZ_{EPMA}, ODZ_{Br} and ODZ_{Cr} are linked to each other and how they evolve with time and temperature.~~

Oxidized thickness distribution

Fig. 5 shows the oxide layer and ODZ_{EPMA} thicknesses measured for L-PBF P600 and ~~EBM~~ E-PBF P600 oxidized 2 000 h at 500 °C and 500 h at 600 °C. Corresponding net mass change per

unit area, oxide layer thickness and ODZ_{EPMA} thickness were presented in a previous work [24]. The ratio $\frac{\mathbf{ODZ_{EPMA}}\ \boldsymbol{thickness}}{\boldsymbol{OL\ thickness}}$ were calculated for both samples and both conditions. For samples oxidized 500 h at 600 °C, it is 2.7 for ~~EBM~~ E-PBF sample and 3.2 for L-PBF sample. For samples oxidized 2 000 h at 500 °C, this ratio is 44 for L-PBF sample and 46 for ~~EBM~~ E-PBF sample. These results show that the ratio of oxygen diffusion layer thickness and the oxide scale thickness is highly dependent on temperature but independent of the additive manufacturing process.

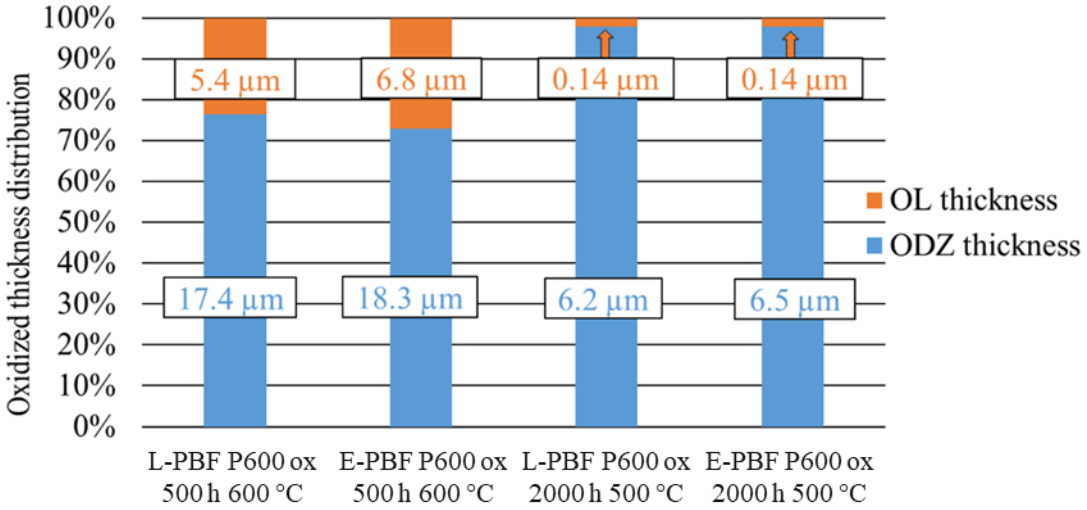

Figure 5: Oxidized thickness distribution of L-PBF P600 and ~~EBM~~ E-PBF P600 oxidized for 500 h at 600 °C and 2 000 h at 500 °C

Evolution of ODZ_{Br} with oxidation conditions

Tensile tests were performed up to rupture on specimens oxidized for 500, 1 000 and 2 000 h at 500 and 538 °C and for 100, 200 and 500 h at 600 °C. For each specimen, fracture surface was observed and ODZ_{Br} was measured. **Fig. 6** shows the evolution of ODZ_{Br} with the square root of time for L-PBF P600, ~~EBM~~ E-PBF P600, L-PBF HIP P600, ~~EBM~~ E-PBF HIP P600 and Cast P600 specimens. It shows that the growth kinetics of ODZ_{Br} ~~follows a~~ are consistent with parabolic ~~law~~ kinetics. Measures of ODZ_{Br} present large error bars which do not allow to observe any significant influence of the microstructure on the ODZ_{Br} thickness for the different Ti-6Al-4V alloys.

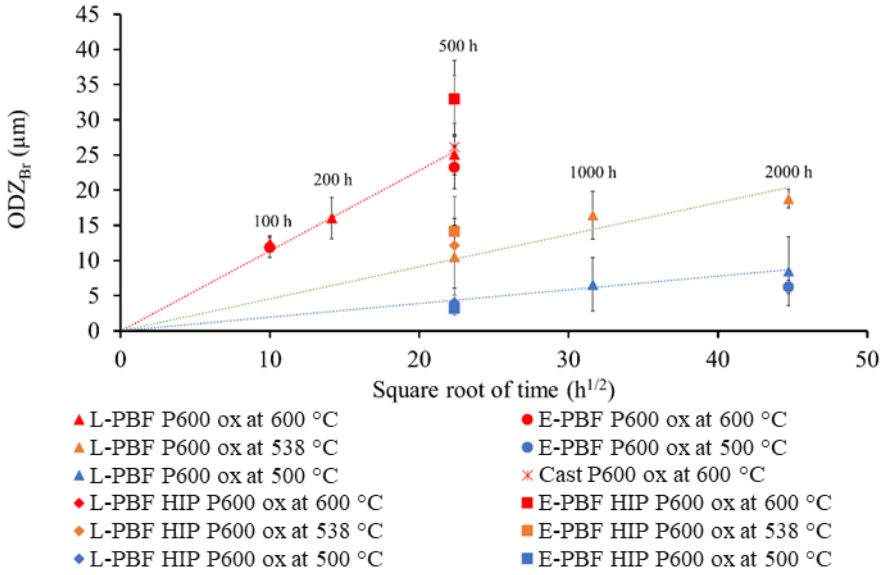

Figure 6: ODZ_{Br} thickness as a function of square root of time and of oxidation temperature for L-PBF, L-PBF HIP, ~~EBM~~ E-PBF, ~~EBM~~ E-PBF HIP and cast alloys with ground surfaces with P600 paper.

Evolution of ODZ_{Cr} with oxidation conditions

Open cracks depth were measured all along each specimen. **Fig. 7** shows the evolution of ODZ_{Cr} with the square root of time for L-PBF P600, ~~EBM~~ E-PBF P600, L-PBF HIP P600, ~~EBM~~ E-PBF HIP P600 and Cast P600 specimens. It is observed that the growth kinetics of ODZ_{Cr} ~~follows a parabolic law~~ are consistent with parabolic kinetics. Once again, measures of ODZ_{Cr} present large error bars, so that no significant influence of the microstructure can be observed when comparing the ODZ_{Cr} of all the Ti-6Al-4V alloys for a same oxidation condition.

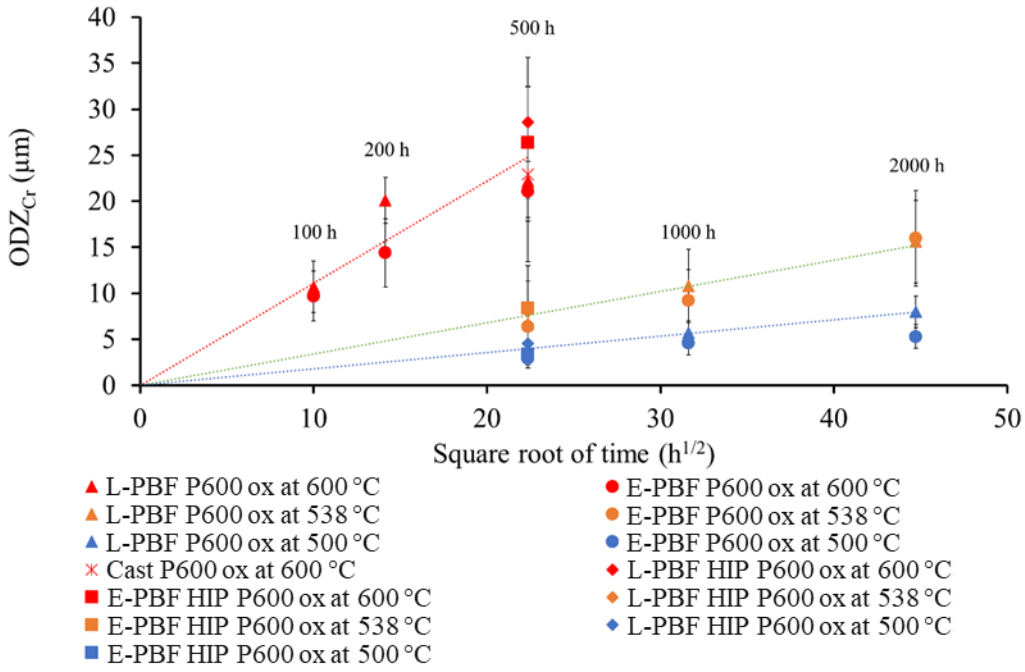

Figure 7: ODZ_{Cr} thickness as a function of square root of time for oxidation at 500, 538 and 600 °C of L-PBF, L-PBF HIP, ~~EBM~~ E-PBF, ~~EBM~~ E-PBF HIP and cast samples with polished P600 surface.

Discussion

Evolution of parabolic constant of ODZ_{Br} and ODZ_{Cr} with the temperature

Fig. 6 and 7 show that both ODZ_{Br} and ODZ_{Cr} can be described with a parabolic law. Therefore, for each temperature, parabolic constants $k'_{p_{ODZ_{Br}}}$ and $k'_{p_{ODZ_{Cr}}}$ were determined. Evolution of both $k'_{p_{ODZ_{Br}}}$ ($m^2.s^{-1}$) and $k'_{p_{ODZ_{Cr}}}$ ($m^2.s^{-1}$) with the temperature are presented in an Arrhenius plot, **Fig. 8.** This plot shows that both parabolic constants follow an Arrhenius law **Eq. 3 and 4** with similar activation energies of 219 +/-80 $kJ.mol^{-1}$ and 220 +/-50 $kJ.mol^{-1}$, respectively. Errors were estimated using the extreme values of parabolic constants in **Fig.8** considering the error bars. Errors in **Fig.8** were estimated from the error in **Fig. 6** and **7**.

$$k'_{p_{ODZ_{Br}}} = 5.8.10^{-3} \cdot exp\left(-\frac{219000 +/-80000}{R \cdot T}\right) \qquad \text{Eq.3}$$

$$k'_{p_{ODZ_{Cr}}} = 4.9.10^{-3} \cdot exp\left(-\frac{220000 +/-50000}{R \cdot T}\right) \qquad \text{Eq.4}$$

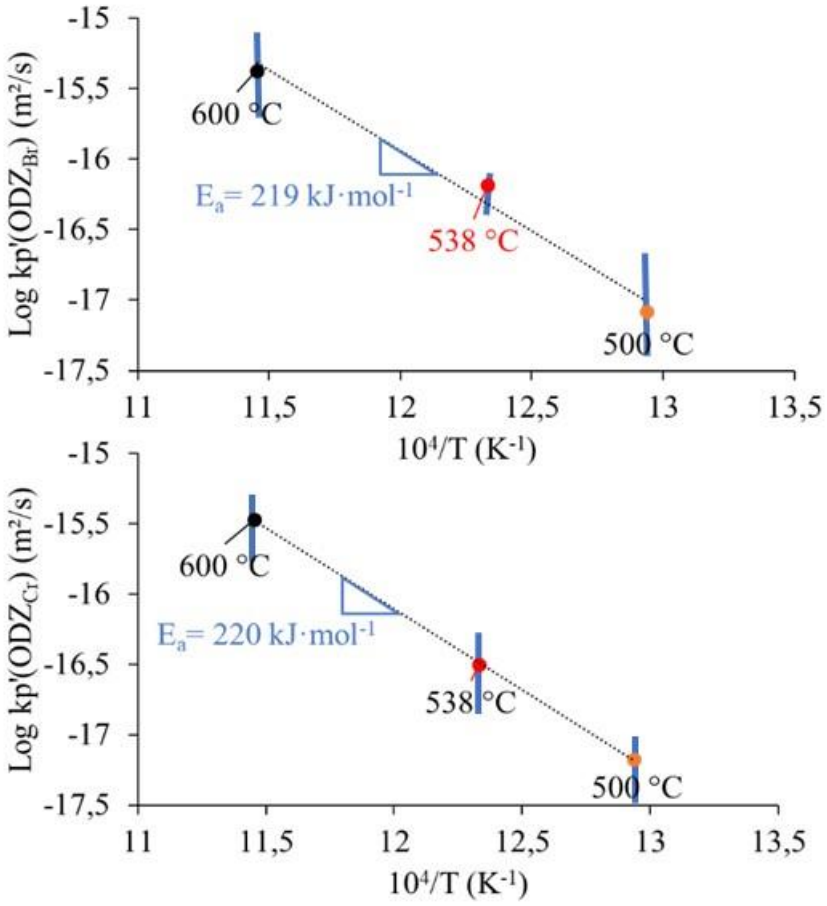

Fig 8: Arrhenius plot showing the evolution of $k'_{p_{ODZ_{Br}}}$ and $k'_{p_{ODZ_{Cr}}}$ with temperature

Modelling of ODZ_{Br} and ODZ_{Cr} with raw data

Arrhenius law parameters determined previously were used in **Eq.5 and Eq.6** in order to model the evolution of ODZ_{Br} and ODZ_{Cr} with the temperature and the time in the temperature domain [500 – 600 °C] and the oxidation duration domain [0 – 2000 h].

$$ODZ_{Br} = \sqrt{5.8 \times 10^{-3} \times e^{-\frac{219\,000+/-80000}{RT}} \times t} \quad \text{Eq. 5}$$

$$ODZ_{Cr} = \sqrt{4.9 \times 10^{-3} \times e^{-\frac{220\,000+/-50000}{RT}} \times t} \quad \text{Eq. 6}$$

with ODZ_{Br} and ODZ_{Cr} in m, t in s, R=8.32 kJ/mol and T in K.

Comparison of ODZ_{Br} and ODZ_{Cr} with ODZ_{EPMA}

ODZ_{Br} and ODZ_{Cr} where compared to the ODZ_{EPMA} in order to establish the relationship between the mechanically affected zone by the environment and the oxygen diffusion in the metal. Three characterisation methods were used to measure the diffusion of oxygen in the metal and the associated mechanically affected zone. ODZ_{Br} and ODZ_{Cr} were compared to ODZ_{EPMA} in **Figure 9,** and a linear relationship was found with correlation coefficients of 0.91 and 0.9, respectively. ODZ_{Br} is 1.5 times larger than ODZ_{EPMA} and ODZ_{Cr} is 1.3 times larger than ODZ_{EPMA}. Taking into account the error bars, we can state that the $\frac{\mathbf{ODZ_{Br}}}{\mathbf{ODZ_{EPMA}}}$ ratio varies from 1.3 to 1.7 and $\frac{\mathbf{ODZ_{Cr}}}{\mathbf{ODZ_{EPMA}}}$ ratio varies from 1.0 to 1.6.

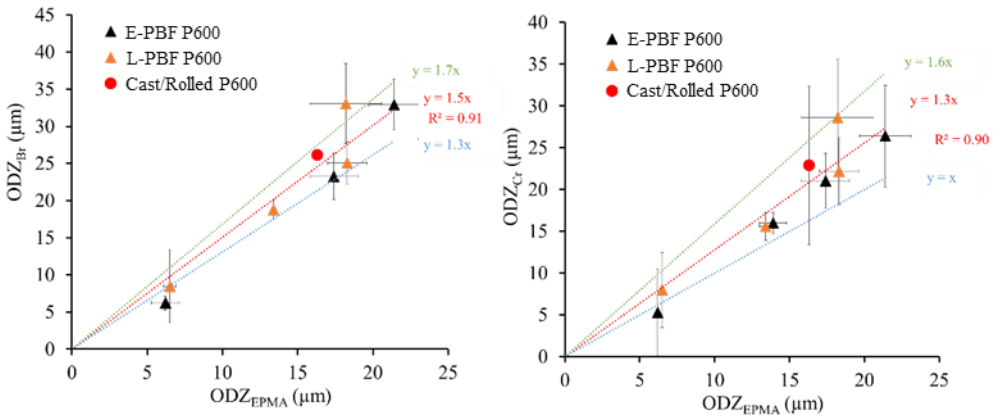

Figure 9: Comparison of ODZ_{Br} and ODZ_{Cr} with ODZ_{EPMA}

These results confirm that the formation of cracks and the brittle rupture correspond to the oxygen diffusion zone. Moreover, **Figure 5** shows that the ODZ thickness is 2.7 to 44 times thicker than the oxide layer thickness depending on oxidation conditions for both AM processes. The ratio of thicknesses $\frac{\mathbf{ODZ}}{\boldsymbol{OL}}$ is larger at lower temperatures, i.e. at temperatures of use of alloy Ti-6Al-4V. At very high temperatures for Ti-6Al-4V alloy, the ratio decreases because the oxide layer growth becomes linear due to the formation of multiple layers in the oxide scale [29]. Embrittlement of Ti-6Al-4V alloy is due to oxidation and is mostly due to the formation of the ODZ compared to the formation of an oxide layer.

Modelling of ODZ_{Br} and ODZ_{Cr} with the effective diffusion coefficient of oxygen D

A review of available literature data of oxygen effective diffusion coefficients in Ti-6Al-4V alloy was shown in Fig.12 of reference [24]. All the data could be fitted with an Arrhenius law between 500°C and 1100°C with an activation energy of -219 kJ/mol. In the present work, both ODZ_{Br} and ODZ_{Cr} activation energies are similar to the activation energy of diffusion of oxygen in the metal. It can therefore be assessed that the extent of brittle rupture area and the formation of cracks are controlled by the diffusion of oxygen in the metal.

Thanks to the ratio found between ODZ_{EPMA}, ODZ_{Br} and ODZ_{Cr} in **Figure 9** and the equation used to determine $\boldsymbol{ODZ_{EPMA} = 4.0 \times \sqrt{(Dt)}}$, with $D = \mathbf{4.0 \times 10^{-4} \times e^{-\frac{219\,000}{RT}}}$ ($m^2.s^{-1}$) [24], ODZ_{Br} and ODZ_{Cr} can be calculated using **Eq.7 and 8**, for temperature between 500 and 600 °C and for durations between 0 and 2 000 h, i.e. they can be written as a function of D, the oxygen diffusion coefficient of oxygen in the Ti-6Al-4V metallic matrix.

$$\boldsymbol{ODZ_{Br} = 6.0 \times \sqrt{(Dt)} = \sqrt{1.4 \times 10^{-2} \times e^{-\frac{219\,000}{RT}} \times t}} \quad \text{Eq.7}$$

$$\boldsymbol{ODZ_{Cr} = 5.2 \times \sqrt{(Dt)} = \sqrt{1.1 \times 10^{-2} \times e^{-\frac{219\,000}{RT}} \times t}} \quad \text{Eq.8}$$

with ODZ_{Br} and ODZ_{Cr} in m, t in s, D in m^2/s, R=8.32 kJ/mol and T in K.

Vaché *et al.* proposed the same parabolic model for the ODZ growth kinetics in Ti-6Al-4V alloys, but with different parameters Eq. 9 and 10 [30]. These models were based on data from literature mainly obtained by microhardness measurements, for temperatures between 500 and 700 °C and durations between 0 and 30 000 h.

$$\boldsymbol{ODZ_{OAZ-Ti64} = 2.8 \times \sqrt{3.83 \times 10^{-5} \times e^{-\frac{199850}{RT}} \times t}} \quad \text{Eq. 9}$$

$$\boldsymbol{ODZ_{Br-Ti64} = 3.4 \times \sqrt{3.83 \times 10^{-5} \times e^{-\frac{199850}{RT}} \times t}} \quad \text{Eq. 10}$$

With ODZ_{Br} and ODZ_{Cr} in m, t in s, R=8.32 kJ/mol and T in K. ODZ_{Br} and ODZ_{Cr} were modelled with 3 different methods. For each model, the corresponding parabolic constants $\boldsymbol{k'_{p_{ODZ_{Br}}}}$ and $\boldsymbol{k'_{p_{ODZ_{Cr}}}}$ were determined. In **Fig. 10** the parabolic constants of all three models for ODZ_{Br} and ODZ_{Cr} are compared in an Arrhenius plot. Each parabolic constant was calculated every 50 °C in their temperature range of validity only. Parabolic constants were also compared to those calculated from the criteria $\boldsymbol{ODZ_{EPMA} = 4.0 \times \sqrt{(D_{lit} t)}}$ used in a previous work [24]. **Figure 10** shows that all models are quite similar in the temperature range 500 – 600 °C.

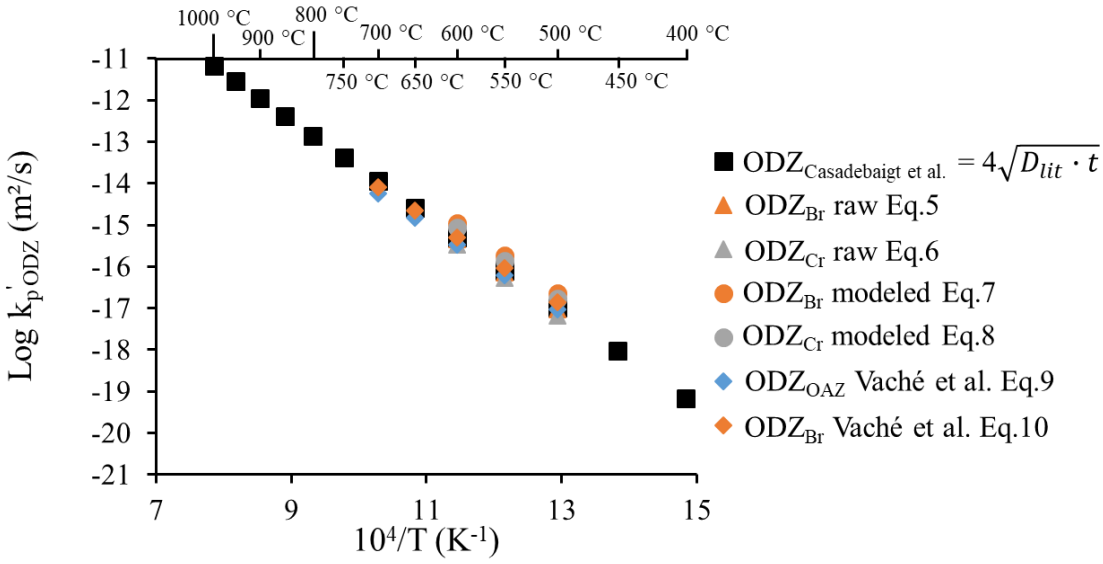

Figure 10: Evolution of ODZ with temperature calculated with models presented in Eq.5 to 10

In the preceding, the formation of ODZ_{Br} and ODZ_{Cr} was only discussed with regard to the presence of oxygen. However, nitrogen has strenghtening and embrittlement effects higher than oxygen for titanium alloys [7]. Chaze *et al.* **[31]** and Dupressoire *et al.* **[32]** showed that nitrogen influenced oxidation mechanisms of titanium alloys and reduced the ingress of oxygen in the metal. Sadly, not enough works were devoted to nitrogen diffusion in titanium, and not enough data are available to compare the activation energies of oxygen and nitrogen diffusion with the growth kinetics of the embrittled zone. Nevertheless, it was shown that oxygen diffuses much deeper in the alloys than nitrogen [33, 34], and the present work shows a high consistency between the oxygen diffusion coefficient and the embrittlement kinetics.

Conclusion

Tensile tests were performed on L-PBF P600, ~~EBM~~ E-PBF P600, L-PBF HIP P600, ~~EBM~~ E-PBF HIP P600 and Cast P600 specimens oxidized for 100 to 2 000 h at 500 to 600 °C. Oxygen embrittlement was characterized by the parameter $ODZ_{Br,}$ related to the brittle rupture surface and by the parameter ODZ_{Cr} related to the area with cracks, which were measured on each specimen. No significant influence of microstructure on oxygen embrittlement was observed despite the large differences of laths thicknesses between, for example, the annealed L-PBF samples (0.5 µm) and the HIPped L-PBF samples (2.5 µm), i.e. an interfaces density 5 times higher for the annealed non-HIPped samples.

Observation of ruptured tensile specimens showed a brittle rupture mode and the presence of cracks in the oxygen diffusion zone. The ODZ was found to be 2.7 to 44 times thicker than the oxide layer, depending on oxidation conditions. Activation energies of growth of the ODZ_{Br} and $ODZ_{Cr,}$ were determined in this work. They were found to be very close to the one for the growth of ODZ_{EPMA}, showing that brittle rupture surfaces and cracks lengths are very likely to be controlled by the diffusion of oxygen in the alpha-phase of the metal. A proportionality of 1.5 and 1.3 with ODZ_{EPMA} defined as $\boldsymbol{ODZ_{EPMA} = 4 \cdot \sqrt{(D \cdot t)}}$ was observed with ODZ_{Br} and ODZ_{Cr} respectively, for oxidation durations of 0 to 2000 h and temperatures between 500 and 600 °C. Therefore, ODZ_{Br} and ODZ_{Cr} can be modelled very easily using the effective diffusion coefficient of oxygen and the criteria $\boldsymbol{ODZ_{Br} = 6.0 \cdot \sqrt{(D \cdot t)}}$ and $\boldsymbol{ODZ_{Cr} = 5.2 \cdot \sqrt{(D \cdot t)}}$, respectively, and independently of the microstructure of the Ti-6Al-4V alloy.

Acknowledgments

This work performed at CIRIMAT laboratory falls within the framework of the Andduro project hosted by the French Institute of Technology IRT Saint Exupery, supported by the Occitanie Region and industrial partners. The authors gratefully acknowledge Claudie Josse, Sophie Gouy (UMS Castaing, Toulouse, France) for their technical assistance on FIB cross-section observations and EPMA measurements respectively, Julien Milanese and Jean-Baptiste Osio (MIDIVAL, France) for their technical assistance on tensile tests.

Data availability

The raw/processed data required to reproduce these findings cannot be shared at this time as the data also forms part of an ongoing study

Bibliography

[1] K.V. Wong, A. Hernandez, A Review of Additive Manufacturing, ISRN Mechanical Engineering 2012 (2012).
[2] W.E. Frazier, Metal Additive Manufacturing: A Review, Journal of Materials Engineering and Performance 23(6) (2014) 1917-1928.
[3] T. Zhang, C.-T. Liu, Design of titanium alloys by additive manufacturing: A critical review, Advanced Powder Materials 1(1) (2022) 100014.
[4] H.K. Rafi, N.V. Karthik, H. Gong, T.L. Starr, B.E. Stucker, Microstructures and Mechanical Properties of Ti6Al4V Parts Fabricated by Selective Laser Melting and Electron Beam Melting, Journal of Materials Engineering and Performance 22(12) (2013) 3872-3883.
[5] B. Vrancken, L. Thijs, J.-P. Kruth, J. Van Humbeeck, Heat treatment of Ti6Al4V produced by Selective Laser Melting: Microstructure and mechanical properties, Journal of Alloys and Compounds 541 (2012) 177-185.
[6] C. Qiu, N.J.E. Adkins, M.M. Attallah, Microstructure and tensile properties of selectively laser-melted and of HIPed laser-melted Ti–6Al–4V, Materials Science and Engineering: A 578 (2013) 230-239.
[7] W.L. Finlay, J.A. Snyder, Effects of three interstitial solutes (Nitrogen, Oxygen and Carbon) on the mechanical properties of high-purity alpha titanium, Journal of Metals 188 (1950) 227-286.
[8] R.I.J. H. R. Ogden, The effects of carbon, oxygen, and nitrogen on the mechanial properties of titanium and titanium alloys, TML Report n°20, 1955.
[9] Y.T. Lee, G. Welsch, Young's modulus and damping of Ti・6Al・4V alloy as a function of heat treatment and oxygen concentration, Materials Science and Engineering: A 128(1) (1990) 77-89.
[10] L. Bendersky, A. Rosen, The effect of exposure on fracture of Ti-6AL-4V alloy, Engineering Fracture Mechanics 13(1) (1984) 111-118.
[11] C.E. Shamblen, T.K. Redden, Air Contamination and Embrittlement of Titanium Alloys, Science, Technology, and Application of Titanium. / Jaffee, R. I. (ed.). Oxford Pergamon Press Ltd. (1970). (1970) 199-208.
[12] W.J. Jia, W.D. Zeng, J.R. Liu, Y.G. Zhou, Q.J. Wang, Influence of thermal exposure on the tensile properties and microstructures of Ti60 titanium alloy, Materials Science and Engineering a-Structural Materials Properties Microstructure and Processing 530 (2011) 511-518.
[13] R.W. Evans, R.J. Hull, B. Wilshire, The effects of alpha-case formation on the creep fracture properties of the high-temperature titanium alloy IMI834, Journal of Materials Processing Technology 56(1) (1996) 492-501.
[14] D. Texier, Q. Sirvin, V. Velay, M. Salem, D. Monceau, B. Mazères, A. Andrieu, R. Roumiguier, B. Dod, Oxygen/nitrogen-assisted embritlement of titanium alloys exposed at elevated temperature in: M.W.o.C. 321 (Ed.) 14th World Conference on Titanium, Nantes (France), 2020.
[15] C. Leyens, M. Peters, D. Weinem, W.A. Kaysser, Influence of long-term annealing on tensile properties and fracture of near-alpha titanium alloy Ti-6Al-2.75Sn-4Zr-0.4Mo-0.45Si, Metallurgical and Materials Transactions A 27(6) (1996) 1709-1717.
[16] M. Berthaud, Étude du comportement de l'alliage de titane Ti6242S à haute température sous atmosphères complexes : applications aéronautiques, 2018.
[17] K.S. Chan, M. Koike, B.W. Johnson, T. Okabe, Modeling of Alpha-Case Formation and Its Effects on the Mechanical Properties of Titanium Alloy Castings, Metallurgical and Materials Transactions A 39(1) (2008) 171-180.
[18] R. Gaddam, M.L. Antti, R. Pederson, Influence of alpha-case layer on the low cycle fatigue properties of Ti-6Al-2Sn-4Zr-2Mo alloy, Materials Science and Engineering: A 599(Supplement C) (2014) 51-56.

[19] A.L. Pilchak, W.J. Porter, R. John, Room temperature fracture processes of a near-Î± titanium alloy following elevated temperature exposure, Journal of Materials Science 47(20) (2012) 7235-7253.
[20] Y. Zhou, S.F. Wen, B. Song, X. Zhou, Q. Teng, Q.S. Wei, Y.S. Shi, A novel titanium alloy manufactured by selective laser melting: Microstructure, high temperature oxidation resistance, Materials & Design 89 (2016) 1199-1204.
[21] Z. Liang, B. Tang, Y. Gui, Q. Zhao, High-Temperature Oxidation Behavior of the Ti-6Al-4V Alloy Manufactured by Selective Laser Sintering, JOM 71(10) (2019) 3600-3605.
[22] T. Fujieda, Y. Cui, K. Aoyagi, Y. Koizumi, A. Chiba, Electron beam melting of boron-modified Ti–6Al–2Sn–4Zr–2Mo–0.1Si alloy with superior tensile strength and oxidation resistance at elevated temperatures, Materialia 4 (2018) 367-372.
[23] A. Casadebaigt, J. Hugues, D. Monceau, Influence of Microstructure and Surface Roughness on Oxidation Kinetics at 500–600 °C of Ti–6Al–4V Alloy Fabricated by Additive Manufacturing, Oxidation of Metals 90(5) (2018) 633-648.
[24] A. Casadebaigt, J. Hugues, D. Monceau, High temperature oxidation and embrittlement at 500-600°C of Ti-6Al-4V alloy fabricated by Laser and Electron Beam Melting, Corrosion Science 175 (2020) 108875.
[25] K.A. Y. Cui, Y. Koizumi, T. Fujieda, A. Chiba, Enhanced oxidation resistance of a titanium-based alloy by the addition of boron and the application of electron beam melting, Additive Manufacturing 31(100971) (2020).
[26] C.O.-M. F. Estupinan-Lopez, C. Gaona-Tiburcio, J. Cabral-Miramontes, R. G. Bautista-Margulis, D. Nieves-Mendoza, E. Maldonado-Bandala, F. Almeraya-Calderon, A. J. Lopes, Oxidation Kinetics of Ti-6Al-4V Alloys by Conventional and Electron Beam Additive Manufacturing, Materials 2023 16(3) (2023) 1187.
[27] K. Dietrich, J. Diller, S. Dubiez-Le Goff, D. Bauer, P. Forêt, G. Witt, The influence of oxygen on the chemical composition and mechanical properties of Ti-6Al-4V during laser powder bed fusion (L-PBF), Additive Manufacturing 32 (2020) 100980.
[28] M. Surand, Étude du comportement viscoplastique en traction et en fluage de l'alliage TA6V de 20 à 600 degrés Celsius, Université de Toulouse, 2013.
[29] H.L. Du, P.K. Datta, D.B. Lewis, J.S. BurnellGray, High-temperature corrosion of Ti and Ti-6Al-4V alloy, Oxidation of Metals 45(5-6) (1996) 507-527.
[30] N. Vaché, Y. Cadoret, B. Dod, D. Monceau, Modeling the oxidation kinetics of titanium alloys: Review, method and application to Ti-64 and Ti-6242s alloys, Corrosion Science 178 (2021) 109041.
[31] A.M. Chaze, C. Coddet, The role of nitrogen in the oxidation behaviour of titanium and some binary alloys, Journal of the Less Common Metals 124 (1986) 73-84.
[32] C. Dupressoire, A. Rouaix - Vande Put, P. Emile, C. Archambeau-Mirguet, R. Peraldi, D. Monceau, Effect of nitrogen on the kinetics of oxide scale growth and of oxygen dissolution in the Ti6242S titanium-based alloy, Oxidation of Metals vol. 87(n° 3-4) (2017) pp. 343-353.
[33] I. Abdallah, C. Dupressoire, L. Laffont, D. Monceau, A. Vande Put, STEM-EELS identification of TiOXNY, TiN, Ti2N and O, N dissolution in the Ti2642S alloy oxidized in synthetic air at 650 °C, Corrosion Science 153 (2019) 191-199.
[34] C. Dupressoire, M. Descoins, A. Vande Put, E. Epifano, D. Mangelinck, P. Emile, D. Monceau, The role of nitrogen in the oxidation behaviour of a Ti6242S alloy: a nanoscale investigation by atom probe tomography, Acta Materialia 216 (2021) 117134.